






How 3D-Printing Is Changing RF Front-End Design for Space Applications

OSCAR A. PEVERINI ¹ (Member, IEEE), **MAURO LUMIA** ¹ (Member, IEEE),
GIUSEPPE ADDAMO ¹ (Member, IEEE), **GIUSEPPE VIRONE** ¹ (Senior Member, IEEE),
AND NELSON J. G. FONSECA ² (Senior Member, IEEE)

(Invited Paper)

¹Istituto di Elettronica e di Ingegneria dell'Informazione e delle Telecomunicazioni, Consiglio Nazionale delle Ricerche, 10129 Turin, Italy

²Antennas and Sub-Millimeter Waves Section, European Space Agency, 2200 AG Noordwijk, The Netherlands

CORRESPONDING AUTHOR: Oscar A. Peverini (e-mail: oscarantonio.peverini@cnr.it).

ABSTRACT 3D-printing is leading to a major transformation in many industrial and application sectors, ranging from medical to aerospace. In the space sector, 3D-printing has firstly been adopted for the development of structural and thermal parts, such as brackets and heat pipes. In more recent years, thanks to improvements in precision and surface roughness, 3D-printing technologies have steadily been investigated also for the development of radio frequency components and advanced payloads. Indeed, the unique features of 3D-printing, including the free-form capability and the ease for customization, make these manufacturing technologies very appealing in the development of complex radio-frequency front-ends for space applications, including New Space constellations and next generation software-defined communication satellites. They also enable a drastic simplification of mechanical designs by reducing the number of interfaces and assembling screws of large radio-frequency front-ends, thus leading to significant mass savings and higher integration. This paper briefly reports on recent advances in 3D-printing that have been carried out according to the current trends in radio-frequency front-ends for satellite communications.

INDEX TERMS MTT 70th Anniversary Special Issue, 3D-printing, additive manufacturing, microwave components, multiple beam antennas, array antennas, communication satellite, new space.

I. INTRODUCTION

Additive Manufacturing (AM), also known as 3D-printing, encompasses several technologies, in which objects are built by adding material layer-by-layer according to digital 3D models. The various AM technologies currently available mainly differ in the process used to solidify materials (*e.g.*, laser melting, or photo-polymerization) as well as the materials themselves (*e.g.*, metal alloys or ceramics). Compared to conventional manufacturing processes, 3D-printing offers the potentiality of building parts quickly and cost-efficiently, thus accelerating development cycles. Additionally, end-products can be optimized and customized for individual or series production. Because of these advantages, additive manufacturing is currently widely applied in different industrial and application sectors, ranging from aerospace to medicine [1]. In the aerospace sector, for example, AM technologies are applied

to build complex, lightweight, and reliable components with almost no waste of material [2]. Since parts can be built on demand rather quickly, overproduction and storage inventory can be almost eliminated. In the medical field, AM enables the production of metal implants for bone reconstruction that can be customized to all body areas [3], which has a great impact in orthopedic oncology.

In the space sector, 3D-printing was initially investigated for developing extremely lightweight and robust structural parts, such as antenna brackets [4]. In more recent years, AM technologies have steadily been investigated also for the development of Radio Frequency (RF) components and payloads. Some simple 3D-printed RF front-ends are even already in orbit. Launched in August 2019, Boeing's AMOS-17 satellite is believed to have the first 3D-printed antenna operating in space, while the mission PolarCube, a 3U CubeSat

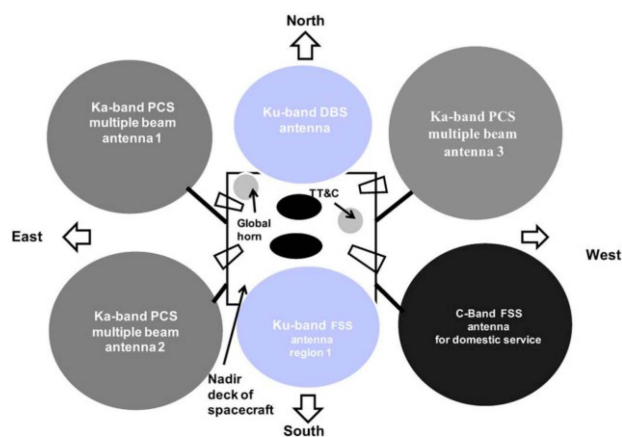


FIGURE 1. Spacecraft layout reported in [6], showing various antennas for multiple satellite services. (©2015 IEEE).

developed by the University of Colorado Boulder and launched in January 2021, embarked a 118.75 GHz 3D-printed corrugated horn [5]. The number of 3D-printed RF front-ends in space is expected to grow exponentially in coming years as satellite manufacturers and microwave payload sub-system providers are turning to the technology and investing in related research and development activities with focus on more advanced equipment to address the needs of future space systems.

This paper reports on the current trends in RF front-ends for communication satellites (Section II), which rely on very dense arrays of antenna-feed chains on board of large satellite platforms or on simple antenna architectures embarked on small satellites (*e.g.*, cubesats) of large constellations (up to thousands of satellites). On the basis of the main benefits provided by AM in this application domain, the most relevant 3D-printing technologies are briefly reviewed and compared to standard machining (Section III). Hence, the main outcomes of the studies carried on the applicability of AM to the development of stand-alone RF components for space are reported (Section IV-A). The most relevant advantage coming from AM is the integration of different RF functionalities in a single mechanical part, for which some examples are briefly discussed (Section IV-B). Finally, two examples of very complex RF front-ends developed through 3D-printing are reviewed (Section IV-C), before some words of conclusion and future perspectives in Section V.

II. CURRENT TRENDS IN RF FRONT-ENDS FOR COMMUNICATION SATELLITES

The complexity of RF payloads for communication satellites have steadily increased throughout the past decades with the introduction of new services and the use of higher frequencies for commercial, military, and civil applications, among which are Fixed Satellite Services (FSS), Direct Broadcast Satellite (DBS) services, Personal Communications Services (PCS), Mobile Satellite Services (MSS), and Inter-Satellite Services (ISS) [6]. These services require the availability of

communication links between the satellite and ground stations, user terminals, other satellites, and/or moving platforms such as aircrafts and ships. Fig. 1 shows the layout of a typical Geostationary Earth Orbit (GEO) spacecraft considered nowadays to replace older satellites reaching end-of-life and combining the continuity of more established services (*e.g.*, FSS, DBS) with the introduction of newer services (*e.g.*, PCS) [6]. The latter require accommodating more antennas having advanced front-ends, resulting in stringent requirements particularly on mass and volume without compromising RF performance.

In the area of GEO satellite communication, High Throughput Satellites (HTS) and Very High Throughput Satellites (VHTS) with aggregate capacity of hundreds of Gbps and up to Tbps are required to meet the increasing data traffic demands. As an example, Eutelsat Ka-Sat, launched in 2010, provides a coverage over Europe with an aggregate capacity of 90 Gbps distributed over 82 beams [7]. To achieve high data rates, while reducing the cost per Gbps at profitable costs around 1 MEuro/Gbps when considering both the ground and space segments [7], [8], several technological solutions have been identified in recent years.

- 1) As in terrestrial mobile networks, space diversity can be adopted to re-use physical-level resources, like frequency and polarization. This is achieved by dividing the region of interest in several spots (*i.e.*, cells) that are illuminated by dedicated antenna beams. Beams corresponding to adjacent spots use different colors (*i.e.*, different frequency sub-bands and/or polarization states) to minimize inter-channel interference. A four-color scheme ($N = 4$) is typically implemented, for which the available band is sub-divided in two or four sub-bands, depending on whether polarization discrimination is adopted or not (Fig. 2). The repetition of the elementary set of beams with different colors over the service area determines the increase in aggregate capacity at satellite level. Thus, the total number of beams is a key parameter to reach very high throughput and drives the complexity and size of RF front-ends [9]. Future VHTS antenna sub-systems are expected to produce several hundreds and even up to a few thousand beams [10].
- 2) Throughput can be increased by adopting digital modulation schemes with higher spectral efficiency [11]. This solution, in turn, requires higher Equivalent Isotropic Radiated Power (EIRP), which is proportional to the transmitted power and the antenna gain, provided the system is not restricted by power flux density regulations on ground for the downlink. Higher antenna gains can be implemented through narrow spot beams with a Half-Power Beam Width (HPBW) down to 0.2° - 0.3° .
- 3) The feeder links between the satellite and the gateways can be operated in the Q/V bands, thus allocating all the available bandwidth in K/Ka bands to the user links [12] (Fig. 2). This requires RF front-end designs with broadband operation, possibly combining transmit (Tx) and receive (Rx) bands.

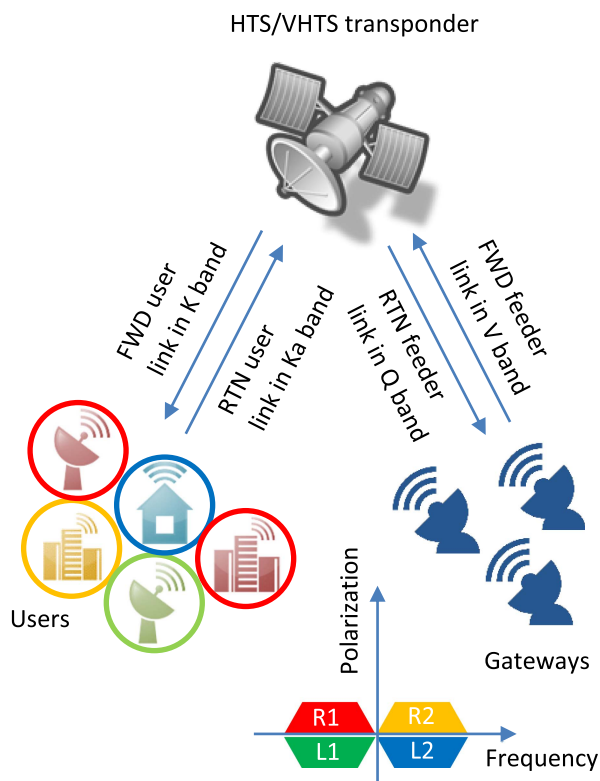


FIGURE 2. HTS/VHTS system based on a star-network architecture with feeder links in Q/V bands and four-color reuse scheme.

- 4) Reconfigurable RF front-ends can add flexibility in redistributing power and bandwidth according to a pre-defined beam-hopping allocation scheme [13] or even to the real-time users' distribution over the geographical region of interest, thus minimizing the difference between the required and offered capacity values [14]. To equalize at best the required and offered capacities, non-regular coverage can also be implemented by tailoring the beam contours on the basis of the users' distribution in the coverage area [15].

All the aforementioned technical solutions ask for Multi-Beam Antennas (MBAs) and corresponding RF front-ends, which can generate a number of simultaneous independent beams. MBAs can be mainly subdivided in three categories.

Array-Fed Reflector (AFR) antennas in Single-Feed-Per-Beam (SFPB) configuration consist of three or four reflectors, each one being illuminated by a cluster of individual feed chains [16]. This is, for example, the antenna system used for Ka-band PCS in Fig. 1. In this configuration, each beam is generated by a dedicated dual-band (Tx/Rx) feed chain. With a four-reflector antenna farm, all the feed chains of the same cluster operate typically at the same color (*i.e.*, same frequency sub-band and polarizations state).

AFR antennas in Multi-Feed-Per-Beam (MFPB) configuration include one or two reflectors illuminated by an array of feed chains. In this configuration, each beam is synthesized by a small set of feed chains connected to a Beam-Forming

Network (BFN), and adjacent beams share some feeds. Active beam forming allows for the dynamic control of the beam sub-array excitation coefficients, thus introducing reconfigurability of the provided coverage. The higher the number of feeds used to synthesize each beam, the higher the degree of reconfigurability [14].

In Direct-Radiating Array (DRA) antennas, two arrays of radiating elements (one for Tx and one for Rx) with the associated BFN directly generate the spot beams [14]. Typically, this solution is adopted in Medium Earth Orbit (MEO) and Low Earth Orbit (LEO) satellite communication, where lower antenna gain is required because of the lower altitudes with respect to GEO systems, leading to reasonable array dimensions. The lower altitude is beneficial for achieving lower propagation delays that are of the utmost importance in low-latency broadband internet applications. To avoid the appearance of grating lobes in the Field of View (FoV) of the antenna (as large as $\pm 55^\circ$), radiating apertures as low as half-wavelength may be required. In this case, higher integration of the RF front-end is essential. Active beamforming may allow for beam reconfigurability over the full antenna FoV.

For GEO satellite systems, the gain and spatial selectivity requirements would lead to a physically large DRA beyond the reach of currently available technology and launcher's capabilities. For these reasons, reconfigurable GEO satellites under development mostly rely on imaging array configurations, the preferred configuration being single-offset reflector geometries where all feeds contribute to all beams [17]. These antenna solutions bring challenges to the beamforming stage, as the computational effort is also "magnified" by the optics [18]. These configurations lead to feed clusters with a number of elements which is typically less than the number of beams to produce, but still in the order of a few hundreds, thus requiring some innovation to achieve acceptable mass and volume. Imaging array configurations combined with large deployable reflectors are well suited to produce a regional coverage with high spectral density, often referred to as Ultra-High Throughput Satellite (UHTS) systems. DRAs and imaging arrays are the preferred solutions for future fully-reconfigurable software-defined payloads.

For a given mission scenario, the specific advantages and disadvantages of the MBA solutions with the associated front-ends have to be carefully traded-off in terms of performances (*e.g.*, directivity, C/I, system capacity), power requirements, hardware complexity, reliability, redundancy, reconfigurability, accommodation (*i.e.*, mass, envelope, number and size of reflectors), and costs. The comparison among different MBAs for some relevant mission scenarios are reported in [9], [14], [15]. As an example, Viasat-3, a global system comprising three GEO satellites and expected to be launched early 2023, is anticipated to deliver at least 1 Tbps per satellite, each with a coverage having more than 2000 beams (Fig. 3), leading to new challenges in terms of signal processing and resource management [19]. The antenna system on board of each satellite is likely an imaging array configuration comparable in complexity to the one described in [18], having a reflector

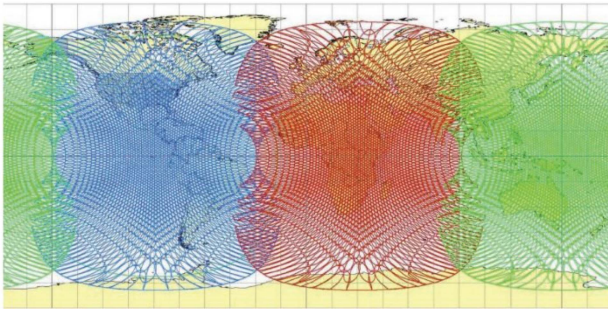


FIGURE 3. Global coverage of the VHTS system Viasat-3, each color corresponding to the service area of a satellite with more than 2000 beams [19]. (©2019 IEEE).

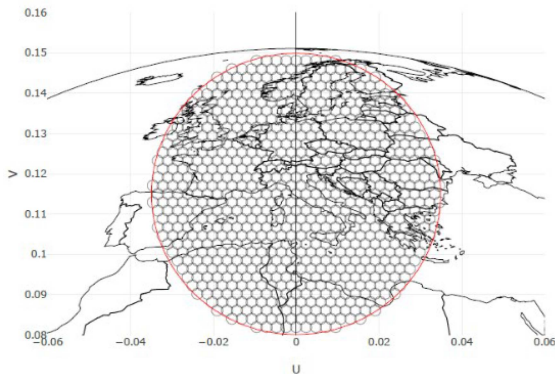


FIGURE 4. Regional coverage of a UHTS system envisioned for future 5G mobile direct services with around 1000 beams across Europe [20].

of 3 m in diameter or larger and a feed system of about 500 elements, in line with current onboard processor capabilities. The typical beam diameter of these satellites with global coverage is in the order of 0.5° or larger. Future UHTS systems will require even smaller beam diameters, typically in the order of 0.3° and less [10]. The regional coverage in Fig. 4, envisioned for future 5G mobile direct services with non-terrestrial networks [20], comprises around 1000 beams of about 0.16° in diameter across Europe, which is more than a factor 10 improvement when compared to the 82 beams of the existing Ka-Sat system. The corresponding antenna systems would need larger reflector apertures, typically around 8 m in diameter, only possible using large deployable reflector technology [21], and large feed arrays, in the order of 2 m in diameter, with several hundreds of elements.

On the extreme opposite, mega-constellation satellites require much less beams per satellite, as the very high total throughput is achieved at system level rather than at satellite level. For example, the first generation OneWeb satellites produce only 16 user-beams each. But since the final constellation will have over 600 satellites, the complete system will still produce up to 10000 beams. Even with these simpler RF front-ends, innovative manufacturing solutions are required to bring the cost down and make them compatible

with the relatively large productions required compared to space sector standards. This drastic evolution of space systems led to a paradigm shift, further amplified by the emergence of a commercially driven New Space sector, which resulted in the introduction of Design For Manufacture and Assembly (DFMA) ideas into a historically conservative industry. In addition, the use of system level design methodologies, such as Model-Based Design (MBD), and progress in multi-physics simulation enabled to relax unnecessarily demanding specifications at sub-system level. All these aspects contributed to form a suitable environment for the introduction of alternative manufacturing technologies in the space sector.

III. 3D-PRINTING TECHNOLOGIES FOR RF SPACE APPLICATIONS

From the previous overview, it can be understood that the satellite communication market is evolving towards medium-volume production of antennas and associated front-ends. Indeed, in GEO applications, dense and complex focal planes of hundreds of feed chains and BFNs (possibly with distributed amplifiers) are required to implement Tbps VHTS systems. In LEO and MEO applications, constellations of several tenths, hundreds, or even thousands of low-cost small satellites have to be deployed, as in the case of Starlink, OneWeb and Kuiper mega constellations [22]. As a consequence, the satellite industry requires a change in how antennas and RF front-ends are manufactured, assembled, and tested [23].

In this framework, additive manufacturing technologies are being steadily investigated and exploited for the development of RF equipment for satellite communication payloads at component and sub-system levels. Indeed, AM technologies provide several advantages with respect to conventional machining (*e.g.*, turning, milling and electrical discharge machining), among which are free-form capability, fit-for-purpose design, screwless near-net shapes, lower lead time and costs [24]. The free-form capability is related to the property of the AM processes, according to which the building effort is almost the same for canonical or more complex shapes, retaining the same volume. In 3D-printing processes, parts are built by adding material instead of subtracting material from solid blocks. In this way, parts do not need to be designed to guarantee the access of machining tools to the surfaces of the internal channels. This aspect translates in a design-for-purpose approach, where parts may be optimized for the required functionalities. Additionally, components do not need to be split in several mechanical parts that are individually machined and then assembled. This property allows for the manufacturing of sub-assemblies implementing several RF functionalities in a single mechanical part, sometimes referred to as a “monolithic” design. Therefore, the number of flanges can be minimized, which is beneficial for high-power applications, where passive intermodulation products can arise at interfaces. Moreover, integration of RF functionalities in a single mechanical part simplifies the assembling and testing procedures. Finally, the use of screws or alignment

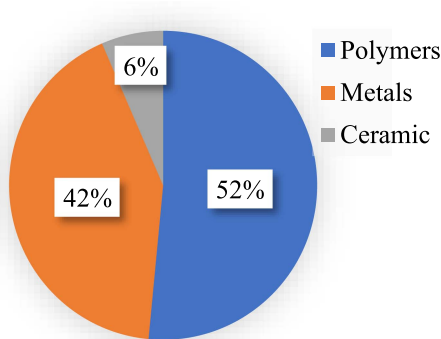


FIGURE 5. Materials used in AM technologies for RF components (survey based on 252 papers in IEEE Xplore Digital Library).

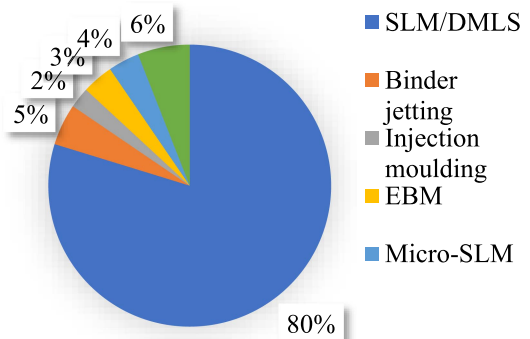


FIGURE 7. Metal-based AM technologies used for RF non-planar components (survey based on 100 papers in IEEE Xplore Digital Library).

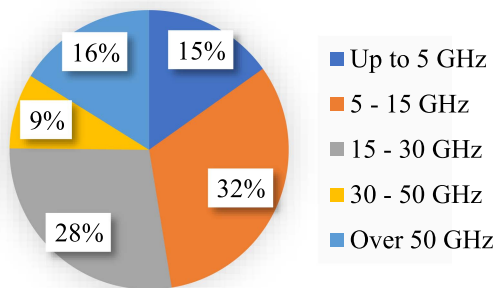


FIGURE 6. Frequency ranges of 3D-printed RF components (survey based on 252 papers in IEEE Xplore Digital Library).

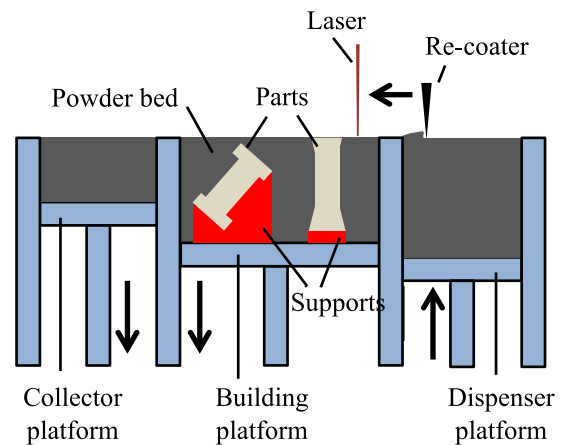


FIGURE 8. Laser powder bed fusion system (sketch from [26]) (©2022 Consiglio Nazionale delle Ricerche).

pins to mount the several mechanical parts composing the components is reduced to the interface between parts. Thus, very thin metal layers (as low as 0.5 mm) tracing the waveguide internal channels can be adopted to implement the RF layouts. This property leads to lightweight and compact components, which is a meaningful aspect for mass and envelope reduction in MBA applications.

3D-printing encompasses several manufacturing technologies that differ in the material and the binding process that are used to build the parts layer-by-layer. In 2010, the American Society for Testing and Materials (ASTM) classified the AM processes into seven categories [25]: vat photo-polymerization, material jetting, binder jetting, material extrusion, powder bed fusion, sheet lamination, and direct energy deposition. The materials used in the manufacturing of RF components can be grouped in three categories, namely, metals, polymers, and ceramics. From a survey carried out in the IEEE Xplore Digital Library and considering more than 250 papers focused on 3D printing of RF components, the distribution of the applied materials is shown in the pie chart of Fig. 5, while the corresponding frequency ranges are reported in Fig. 6. In the following, the processes mainly used for microwave non-planar components are briefly revisited.

A. METAL-BASED AM TECHNOLOGIES

The metal-based AM processes used to produce RF non-planar components are reported in the pie chart shown in Fig. 7. The processes mostly used are Selective Laser Melting (SLM) and Direct Metal Laser Sintering (DMLS) that are trademark variants of the Laser Powder Bed Fusion (LPBF) technology. A brief description of this technology is reported in [26] which includes the sketch of the LBFP system shown in Fig. 8. In LPBF, the parts are built by selectively melting layer-by-layer a bed of metal powder through a high energy laser with power up to 1 kW. Each metal-powder layer (with a thickness as low as 0.1 mm) is spread over the building platform through a re-coater. When the laser has melted the metal powder in the regions of interest, the building platform is lowered, and the process is repeated until the complete part is built. At each step, the powder in excess is transferred to the collector platform. When the printing job has been completed, the parts are cleaned from the unprocessed powder, and the complete platform with the parts still attached to it undergo a stress-relieving post-processing in an oven. Finally, the structures used to support any over-hanging surfaces are removed, and the parts are detached from the building platform. To increase the printing rate, multi-laser LPBF systems are

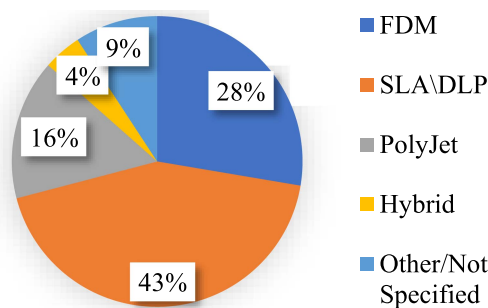


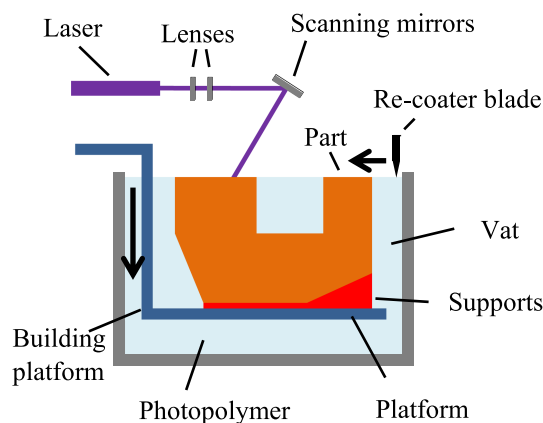
FIGURE 9. Polymer/ceramic-based AM technologies used for RF non-planar components (survey based on 140 papers in IEEE Xplore Digital Library).

commercially available, for which the construction volume can be as high as 80 cm x 40 cm x 50 cm. More detailed information on the LBFP technology is available in [27].

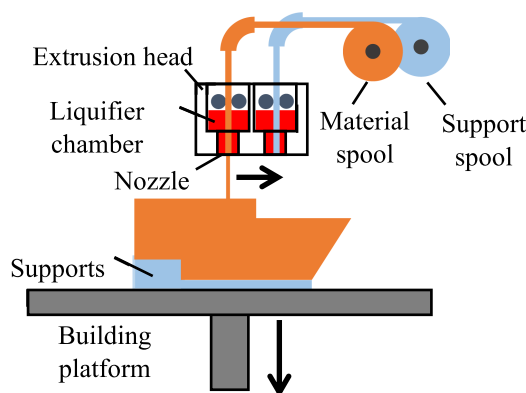
Compared to other metal-based technologies, such as Electron Beam Melting (EBM) [28] or binder jetting [29], the main advantages of the LBFP technology for RF applications is that it can provide parts directly printed in aluminum alloys (such as AlSi10Mg, AlSi7Mg, and Scalmalloy [30]) with good dimensional accuracy (as low as 0.04 mm [31]) and electrical properties. Indeed, for microwave components operating between 10 and 30 GHz, the LPBF technology provides typical values of surface electrical resistivity ranging from 10 to 16 $\mu\Omega\text{cm}$ [32], [33]. This parameter is a combination of the bulk resistivity of the material and the surface roughness. The latter mainly depends on the layer thickness, the building direction of the internal RF channels, and on the powder particle size.

B. POLYMER/CERAMIC-BASED AM TECHNOLOGIES

As shown in the pie chart of Fig. 9, the Stereo-Lithography Apparatus (SLA) and the Fused Deposition Modelling (FDM) processes are the ones mostly used in the 3D-printing of polymer/ceramic-based parts. In the SLA process, a UV laser is used to activate the photo-polymerization of a liquid resin inside a vat (Fig. 10(a)). After solidification of a layer, the platform is lowered inside the vat, and the process is repeated. At each step, additional structures are also printed to support over-hanging surfaces. At the end, the platform is lifted, parts are drained and detached from the platform [27]. The solidification process is completed by UV curing the parts in an oven. Typically, functional parts are built in epoxy resins that provide parts with better accuracy and mechanical properties with respect to acrylates resins, although at a lower building rate. Epoxy resins can be loaded with ceramic particles to achieve a ceramic-polymer composite material with improved mechanical/thermal properties, and higher electrical permittivity. Ceramic materials are usually printed through Digital Light Processing (DLP) which is similar to SLA, but a UV light is used to cure the ceramic-polymer material. The UV light is selectively projected on the layer pixels to be photo-polymerized by a digital projector screen consisting of



(a)



(b)

FIGURE 10. (a) Stereo-lithography apparatus system. (b) Fused deposition modelling system (sketches from [26]). (©2022 Consiglio Nazionale delle Ricerche).

microscopic mirrors. SLA/DLP technologies provide manufacturing accuracy ranging from 20 μm to 60 μm with rather smooth surfaces. The latter property is the main advantage with respect to LBFP. However, for hollow waveguide components, metal plating of the internal channels is mandatory, which can be critical in terms of adhesion, uniformity and long-term stability.

In the FDM process, as shown in Fig. 10(b), a filament of polymer is heated inside a liquefier chamber and dispensed on the building platform through a nozzle [27]. The binding of the extruded material is achieved by residual heat energy, solvents, or wetting agents contained in the filament [24]. The liquefier chamber temperature allows for keeping the material in a molten state without degrading its properties, while the nozzle diameter defines the accuracy (approximately 100-200 μm), the resolution, and the printing rate of the system. A wide range of thermoplastic materials is available for the FDM process [27], among which are Acrylonitrile Butadiene Styrene (ABS), PolyAcetic Acid (PLA), ULTEM, and PEEK. Multi-nozzle systems allow for printing parts consisting of different materials. At the end of the building process, the

TABLE 1. Comparison Among Standard Machining and 3D-Printing Technologies Mostly Used or Investigated to Manufacture RF Components for Space Applications

Process	Milling/turning	Electric discharge machining	Electroforming	LPBF	SLA
Material	6000 series aluminum alloy	6000 series aluminum alloy	copper	AlSi7Mg, AlSi10Mg, Scalmalloy	photopolymer resins
Dimensional accuracy	5 - 20 μm	5 - 20 μm	1 - 5 μm	40 - 80 μm	20 - 60 μm
Surface roughness R_a (arithmetic average roughness)	0.4 - 0.8 μm	0.8 - 1.6 μm	0.4 - 1.0 μm	3 - 8 μm (depending on post surface/coating treatment)	1 - 3 μm
Surface electrical resistivity (10 - 30 GHz)	4 - 6 $\mu\Omega\text{ cm}$	6 - 8 $\mu\Omega\text{ cm}$	3 - 5 $\mu\Omega\text{ cm}$ (with gold passivating layer)	10 - 16 $\mu\Omega\text{ cm}$ (without plating)	plating is mandatory
Melting point (metal) or glass transition temperature (polymer)	650 $^{\circ}\text{C}$	650 $^{\circ}\text{C}$	1083 $^{\circ}\text{C}$	570 - 580 $^{\circ}\text{C}$	60 - 120 $^{\circ}\text{C}$
Coefficient of linear thermal expansion	22 - 24 $\cdot 10^{-6}\text{ K}^{-1}$	22 - 24 $\cdot 10^{-6}\text{ K}^{-1}$	16 - 19 $\cdot 10^{-6}\text{ K}^{-1}$	20 - 24 $\cdot 10^{-6}\text{ K}^{-1}$	60 - 90 $\cdot 10^{-6}\text{ K}^{-1}$
Thermal conductivity	170 - 200 W/m/K	170 - 200 W/m/K	385 - 400 W/m/K	180 - 190 W/m/K	0.1 - 0.3 W/m/K
Density	2.7 g/cm ³	2.7 g/cm ³	8.9 g/cm ³	2.7 g/cm ³	1.1 - 1.6 g/cm ³
Tensile strength	260 - 310 MPa	260 - 310 MPa	200 - 360 MPa	230 - 450 MPa	50 - 90 MPa
Near-net shapes (envelope, mass)	massive	massive	near-net shapes	near-net shapes	near-net shapes
Mechanical layout	split-block, multi-layer	split-block, multi-layer	monolithic	monolithic	pseudo-monolithic
Lead time/cost	medium	medium	high	low	low
TRL	9	9	9	8-9	3-5

necessary supporting structures are removed manually or through a chemical bath.

When considering hollow-waveguide components operating from X to Ka band, SLA/DLP techniques are to be preferred to FDM because of better dimensional accuracy and surface finishing. For lower frequency applications (from L to C band), the latter parameters are less critical. In this case, FDM can be advantageous since it allows for the printing of mechanically and thermally stable polymers, such Carbon-Fiber reinforced PEEK (CF-PEEK).

When exploiting polymer/ceramic AM technologies to develop RF components, the surfaces of the inner channels and of the contacting flanges have to be functionalized through metal coating. To this end, a thin layer (typically, less than 1 μm) consisting of palladium, silver or nickel is chemically deposited on the surfaces [34]. This layer acts as an adhesive layer for a sequent thicker metallization (in the order of 10-150 μm), which is typically based on copper. The Tollen's reaction (silver mirror reaction) is a robust method to deposit a silver activation layer on a variety of polymers [35]. An alternative process relies on silver conductive paints that are spread over the inner surfaces by an airbrush [36]. Depending on the required thickness, the subsequent copper layer can be deposited through an electroless chemical process and/or electroplating [37], [38]. The metal coating has to be as homogeneous as possible and thick enough depending on the operating frequencies.

Peeling and oxidation of the copper layer have to be properly considered.

C. COMPARISON AMONG STANDARD MACHINING AND 3D-PRINTING TECHNOLOGIES

Table 1 reports a comparison among standard machining and 3D-printing technologies that today are mostly used or investigated to manufacture RF components for space applications. To this end, the table lists the main mechanical, thermal and electrical parameters of interest for this application domain. Standard machining includes milling, turning and Electrical Discharge Machining (EDM). All these processes can provide RF parts directly in aluminum alloys (*e.g.*, 6000 series) with high accuracy and good surface finishing along with good mechanical and thermal properties. They have been extensively proven in flight, thus exhibiting the maximum Technological Readiness Level (TRL), equal to 9. However, subtractive manufacturing technologies require split/block or multi/layer layouts that result in massive components.

As reported in Table 1, a possible solution to achieve monolithic components with complex inner shapes is electroforming. This technology provides accurate and near-net-shape components built in copper and gold-passivated. The main drawbacks are the high mass and lead time/costs. In this regard, the LPBF process is a very attractive alternative to develop all-metal monolithic components in aluminum with almost the same mechanical and thermal properties as those

provided by standard machining (e.g., thermal conductivity and tensile strength). Consequently, this technology is already at a space-qualified level, as reported in [30]. On the other hand, dimensional accuracy and surface roughness are the main weak points of the LPBF process. Both these properties can be improved by optimizing the process parameters, such as the beam offset and the scaling factors that accounts for the melt pool geometry and the material shrinkage during laser melting, and by properly orienting the part in the building chamber [31], [39]. Additional post-processing can be applied to improve the surface quality of the as-built parts, including shot-peening, chemical/dry etching, or coating [15], [30].

To obtain AM parts with high accuracy and surface quality, the SLA process has also been largely investigated [40]. For space applications, this technology provides the additional advantage of using photopolymer resins (possibly loaded with ceramic particles), thus obtaining lighter parts because of the reduced material density (at least by a factor of 2). This aspect can be fundamental in future missions where mass is a crucial requirement (e.g., CubeSats). However, these advantages will need to be carefully traded-off against the mechanical and thermal properties of photopolymer resins (such as high coefficient of thermal expansion, low thermal conductivity and tensile strength), and the operative conditions.

IV. 3D-PRINTED COMPONENTS AND RF FRONT-ENDS FOR SPACE

A. STAND-ALONE COMPONENTS

As already introduced, AM technologies can provide several meaningful advantages in the development of RF front-ends for space. However, in the early 2010s, these technologies were almost unexplored for RF applications, and their applicability for space-borne payloads had to be completely assessed in terms of environmental/operational conditions (e.g., power-handling, temperature range, vacuum ambient, vibrations), and RF performance. The latter are mainly related to dimensional accuracy and surface electrical resistivity of the manufactured parts. To assess all these aspects, several feasibility studies have been carried out throughout the past years, some results of which are summarized in [41], [42], [43], [44], [45], [46].

At first, AM technologies have been investigated for the development of stand-alone components relevant to satellite communication payloads, including straight and meander waveguides [47], [48], filters [49], [50], [51], [52], [53], [54], ortho-mode transducers/polarizers [55], [56], [57], [58], [59], and radiating elements, such as helix/quad-ridge antennas [23], [60], [61], and feed horns [57], [62]. Investigations on the multipactor performance of AM components have also been carried out [63]. These studies have highlighted that AM parts can achieve higher power-handling because of the lower secondary emission yield [64] that is exhibited by AM surfaces. This effect does not depend on the material composition or crystal structure, but it results from the higher surface roughness of AM parts.



FIGURE 11. Ku-band spline horn cluster manufactured in aluminum using LPBF [65]. (©2018 Thales Alenia Space, printed by Volum-e, and developed in the frame of a CNES project).

All these design activities and investigations have led to a deeper comprehension of AM technologies' benefits and constraints, resulting in the definition of general design rules of RF components using AM. According to this AM-oriented design approach, some important aspects to be considered to achieve the best dimensional accuracy and surface quality, while guaranteeing feasibility and repeatability of the 3D-printing process, are the followings.

- 1) The stair-case effect caused in the surface profile by the layer thickness depends on the building direction [26].
- 2) Over-hanging down-ward surfaces can warp or, even, collapse during the building process. To minimize this risk, supporting structures are needed for the external surfaces. For the inner waveguide channels, these supports cannot be used, because they can degrade the surface quality or cannot be removed. Therefore, downward surfaces of inner channels shall be designed as self-supporting (i.e., with an appropriate inclination angle [26]).
- 3) The design has to consider the maximum available building volume, the minimum printable gap and wall thickness [42].
- 4) Large parts that lay horizontally on the building platform are more easily subjected to warping after detachment from the platform.

The first RF front-ends in orbit are simple radiating elements, since their simple shape makes them particularly well suited for the use of AM. Moreover, conventional manufacturing of such parts typically leads to significant material waste, which can be drastically reduced through AM techniques. The use of 3D-printing also facilitates the integration of structural elements connecting a cluster of feed horns. Fig. 11 shows a small cluster of Ku-band horns manufactured using SLM [65], for which a mass reduction of 30% is reported.

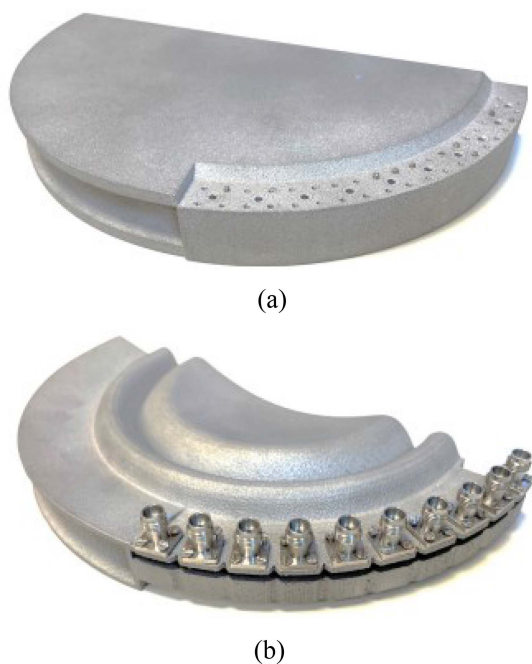


FIGURE 12. Ka-band half-Luneburg geodesic lenses manufactured as a single part using LPBF [66]. (a) Original single-block part. (b) Fully trimmed design.

Similar benefits are demonstrated in [66], reporting on the first quasi-optical front-end, based on a geodesic lens and enabling multiple simultaneous beams, and 3D-printed in a single part using LPBF. The comparison of the design using standard milling and an equivalent 3D-printed design shows a mass reduction of about 30% by removing screws and associated excess material. A further trimming of the excess material, which would require extra work and higher cost with conventional manufacturing techniques, provides a significant mass reduction by a factor of four when comparing the two prototypes reported in Fig. 12.

Filter designs are typically more sensitive to manufacturing tolerances, but they can also benefit from AM techniques. An example of filter layout optimized for 3D-printing is shown in Fig. 13(a). This design is conceived so that the filter can be printed along the longitudinal axis of the main waveguide (from the right to the left), thus allowing to integrate the filter in a feed chain printable along the same direction [51]. This printing direction minimizes losses and dimensional errors, above all in case of dual-polarization systems, while leading to slim feed chains with small footprints. This property is rather relevant in MBA front-ends with very narrow beams, as in the case of sub-wavelength active antennas [30]. Thanks to this arrangement, the measured reflection coefficient of the corresponding prototypes agree well with the predicted one, as shown in Fig. 13(b).

A further example of AM-oriented filter geometry is the one presented in [67], which is a comb-line filter based on triangular waveguide resonators, as shown in Fig. 14(a). The non-canonical triangular waveguide cross-section is selected because it provides inner self-supporting surfaces and,

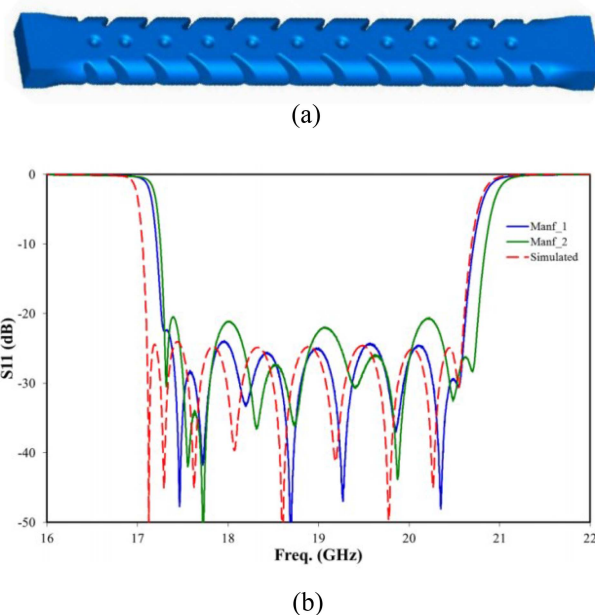


FIGURE 13. Ku-band filter developed in [51] that is optimized for RF front-end integration through 3D-printing. (a) 3D view of the inner waveguide structure. (b) Comparison among predicted and measured reflection coefficients. (©2019 IEEE).

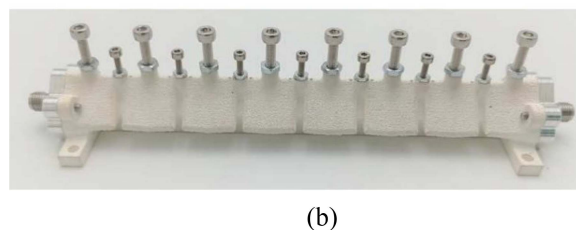
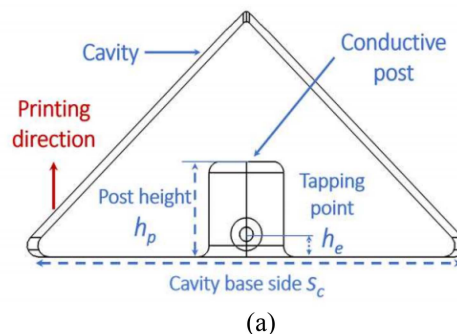


FIGURE 14. Ku-band triangular-waveguide comb-line filter conceived for AM [67]. (a) Cross-section of the waveguide resonator. (b) Prototype manufactured through LPBF in aluminum alloy and copper/silver plated. (©2021 IEEE).

hence, allows for a monolithic manufacturing, thus eliminating the need of any cover. The filter prototype printed through LPBF in aluminum alloy and copper/silver plated is shown in Fig. 14(b). Many other AM-oriented filters have been developed in recent years, as summarized in the review presented in [68].

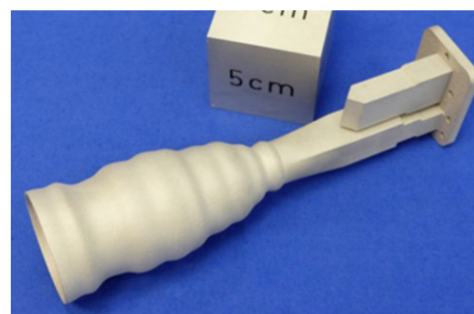
A further lesson learned from the feasibility studies reported in the literature is the need for electromagnetic layouts of the components that shall be robust against dimensional errors, above all for highly resonant components (*e.g.*, filters), phase sensitive parts (*e.g.*, polarizers and phase shifters), and dual-polarization devices (*e.g.*, ortho-mode transducers). An example is the septum-polarizer developed in [58], which is based on two symmetrical septa [69].

B. INTEGRATION OF FUNCTIONALITIES

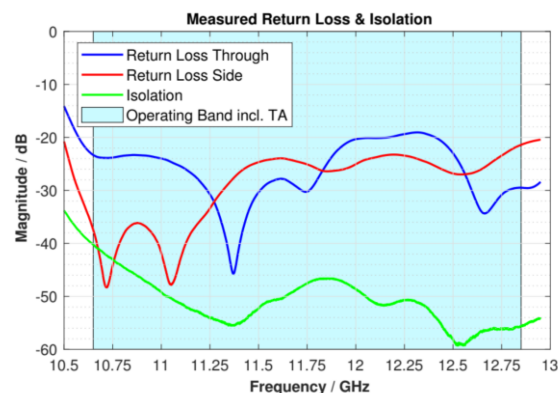
Different AM processes have been investigated and compared in the activities aimed at the development of stand-alone components for space applications. For hollow-waveguide components and antennas, the LPBF process is currently regarded as the most suitable. Indeed, this technology directly provides parts in aluminum alloys with good mechanical and thermal properties (see Table 1). These characteristics make parts printed through LPBF compatible with the harsh space environment. Additionally, the values of dimensional accuracy and electrical surface resistivity provided by this technology allow for the manufacturing of components up to Ka band. For this technology, further studies have been focused on the integration of different functionalities in a single mechanical part. To this end, the AM free-form capability has been exploited as much as possible to achieve significant benefits in terms of mass, envelope, and assembling complexity [70], [71], [72], [73], [74], [75], [76].

As an example, Fig. 15(a) shows the integration of a smooth-wall profile feed-horn with a side-coupling ortho-mode transducer operating in Ku band. Since the electromagnetic model complies with the design rules discussed in Section III-A, the RF performance are compatible with the intended application (*e.g.*, isolation between the input ports below -40 dB). Circular polarization typically requires more advanced ortho-mode transducers. A spline horn combined with a compact E-plane waveguide coupler is also reported in [70]. The innovative E-plane coupler design, which relies on a tandem septum polarizer concept [78], has a single large aperture that proves to be well suited for 3D-printing techniques.

A relevant example of integration of RF functionalities in a monolithic assembly is the K/Ka-band dual-circular polarization feeding network presented in [76]. With reference to the electromagnetic model of Fig. 16(a), this assembly comprises two ortho-mode junctions, four low-pass filters, a waveguide choking section, and two septum polarizers. Its ports 3 and 4 operate in Tx mode at K band, while ports 5 and 6 collect the Rx signal at Ka band. The feeding network is based on a four-fold symmetric architecture, which maximizes the RF performance, above all in terms of port-to-port isolation and spurious higher-order mode excitation. All the building blocks have been designed to allow the assembly printability along its longitudinal axis. This building orientation is essential to minimize manufacturing asymmetries of the waveguide cross-sections, which is fundamental in order not to couple



(a)



(b)

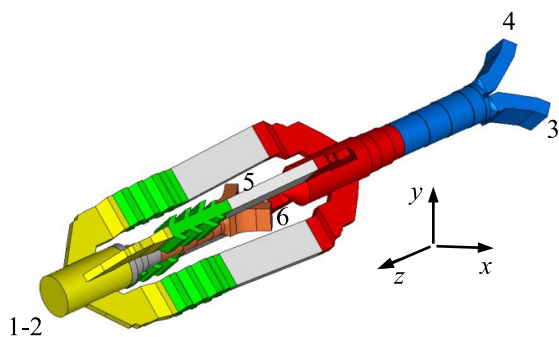
FIGURE 15. Ku-band dual-linear polarization feed chain presented in [70]. (a) Prototype manufactured through LPBF in aluminum alloy. (b) Measured performance. (©2019 Airbus Defense and Space).

degenerate or higher-order modes propagating in the main circular waveguide towards the feed horn.

The prototype manufactured through LPBF in AlSi10Mg alloy, which is shown in Fig. 16(b), exhibits dimensional errors lower than 0.04 mm. To achieve this accuracy, the external shape is designed to reduce deformations caused by thermal stresses arising during the process. To this end, stiffening brackets have been introduced in the regions near the port flanges and the outer K-band waveguide channels. In spite of its complexity, this feeding network can be accommodated in MBAs with a feeding spacing of approximately 40 mm thanks to its slim AM-oriented layout. To highlight the advantages provided by 3D-printing in terms of mechanical complexity, Fig. 16(c) shows an assembly of a K/Ka-band feeding network that is based on the same RF architecture and developed through standard machining. When exploiting novel asymmetrical architectures [79], [80], it is expected that AM technologies will allow for developing very compact configurations of dual-band dual-polarization feed chains compatible with lattice steps of the focal-plane array in the order of 20 mm at K/Ka band.

C. COMPLEX RF FRONT-ENDS

AM technologies may represent a real breakthrough in the area of space RF payloads, if complex and large RF front-ends can be printed in a single mechanical part. In this respect,

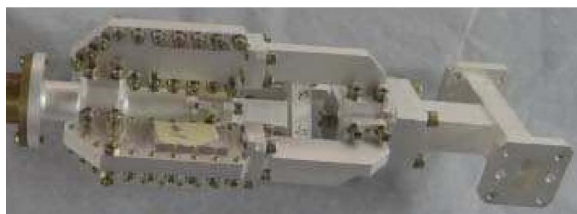


- K-band OMJ # 2
- Low-pass filters
- Circular-waveguide choking
- Ka-band septum-polarizer
- K-band waveguide straights
- K-band OMJ 1
- K-band septum-polarizer

(a)



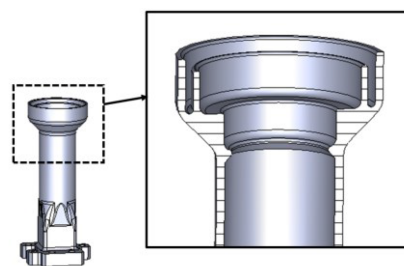
(b)



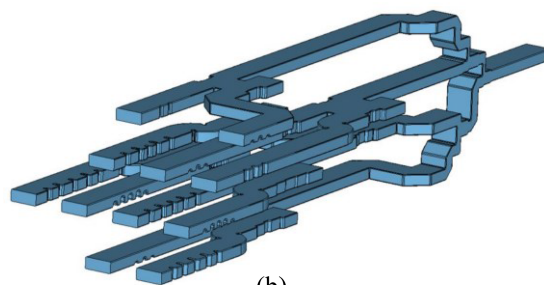
(c)

FIGURE 16. K/Ka-band satcom feeding-network. (a)-(b) Electromagnetic model and prototype printed through LPBF in AlSi10Mg [76]. (©2021 Consiglio Nazionale delle Ricerche and Politecnico di Torino). (c) Assembly based on the same RF architecture and developed through standard machining [77]. (©2017 IEEE).

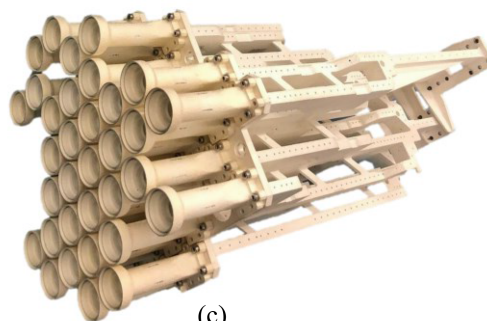
the Authors in [15] have successfully 3D-printed a significant demonstrator for implementing a non-regular coverage of Europe. The coverage asks for 70 non-uniform beams, each one being generated by a set of feed-horns connected to a dedicated sub-BFN. The demonstrator implements the hardware necessary for generating 5 beams, and it consists of 33 feed horns and 5 sub-BFNs. The feed-horns are based on the layout shown in Fig. 17(a), and they are individually manufactured. Instead, the 5 sub-BFNs are printed in a single mechanical



(a)



(b)



(c)

FIGURE 17. 3D-printed multi-beam antenna presented in [15]. (a) CAD of the choked feed horns. (b) 3D view of the inner structure of one sub-beam forming network. (c) Assembled 3D-printed demonstrator consisting of 33 feed horns. (©2022 IEEE).

part. As shown in Fig. 17(b)), each sub-BFN includes E-plane power dividers, H-plane couplers, and phase shifters. The manufactured demonstrator shown in Fig. 17(c) has been printed through LPBF in AlSi10Mg alloy. Subsequently, it has been subjected to surface polishing treatment and to electroless plating with 5- μm thick layer of copper and 0.5- μm thick layer of silver (for passivation). The corresponding surface electrical resistivity is approximately 6 $\mu\Omega\text{cm}$, which makes this technology applicable to complex RF front-ends with demanding requirements in terms of insertion losses.

A further exemplary application of AM technologies to space RF payloads is the cluster of eighteen Ku-band Tx/Rx feed chains reported in [81], [82]. The reference scenario is a multi-spot coverage of the European region with forty beams provided by a three-reflector SFBP antenna. The monolithic cluster manufactured through LPBF in aluminum alloy is shown in Fig. 18(a). This mechanical part implements eighteen array elements, each one consisting of a spline-profile

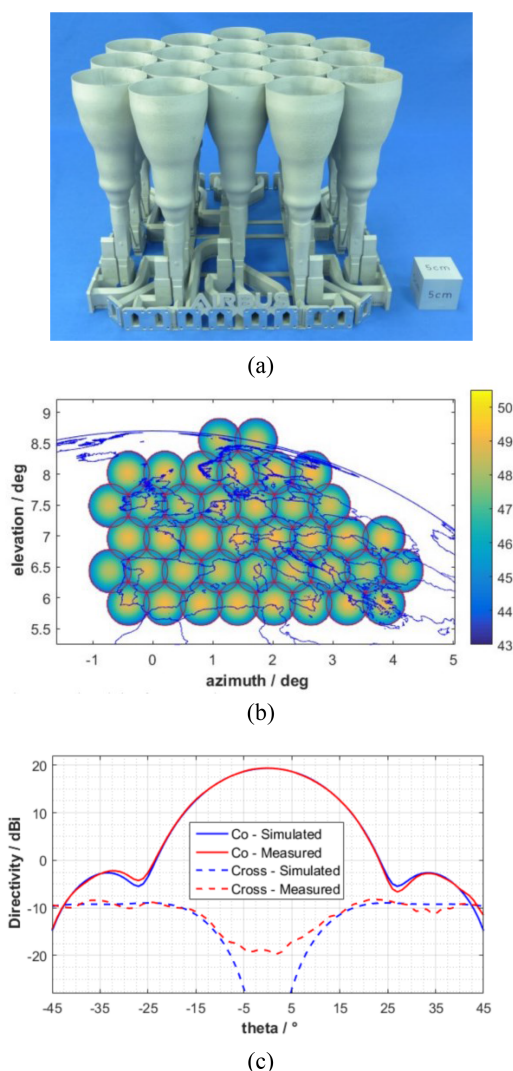


FIGURE 18. Feed cluster for Ku/K band SFPB antennas presented in [81], [82]. (a) Aluminum-alloy assembly printed through LPBF. (b) Multi-beam coverage predicted on the basis of the measured radiation patterns. (c) Comparison between predicted and measured radiation patterns of one feed-cluster element. (©2019 Airbus Defense and Space).

feed horn, a side-coupling ortho-mode transducer, and the waveguide routing necessary to interface the element with the measurement setup. An eighteen-element cluster has been manufactured because its dimensions (191 mm x 392 mm x 305 mm) are compatible with the building volume of the adopted printing system. The cluster weight is approximately 2270 g, thus yielding a reduction of almost 90% with respect to standard machining. The multi-beam coverage predicted on the basis of the measured radiation patterns is shown in Fig. 18(b), while the comparison between predicted and measured radiation patterns of one feed-cluster element is reported in Fig. 18(c).

V. CONCLUSION

Additive manufacturing technologies have already proved to be novel and efficient solutions for the development of either

complex RF front-ends for dense focal planes or very simple cube-sat payloads.

As current AM processes are improved and new ones are placed on the market, including Lithography-based Metal Manufacturing (LMM) or hybrid systems combining 3D-printing and CNC machining, the impact of these technologies in the space sector is envisaged to grow. Consequently, research and training activities on all the aspects of the supply chain, from design to process qualification, are required to make 3D-printing a real breakthrough in the development of space-borne RF payloads.

REFERENCES

- [1] T. T. Wohlers et al., "Part I: Introduction," in *Wohlers Report 2022: 3D Printing and Additive Manufacturing Global State of the Industry*, Fort Collins, CO, USA: Wohlers Assoc. Inc., 2022, ch. 1, pp. 23–52.
- [2] M. Kalender, S. E. Kılıç, S. Ersoy, Y. Bozkurt, and S. Salman, "Additive manufacturing and 3D printer technology in aerospace industry," in *Proc. IEEE 9th Int. Conf. Recent Adv. Space Techn.*, 2019, pp. 689–694.
- [3] J. W. Park and H. G. Kang, "Application of 3-dimensional printing implants for bone tumors," *Clin. Exp. Pediatr.*, vol. 65, no. 10, pp. 476–482, Oct. 2022, doi: [10.3345/cep.2021.01326](https://doi.org/10.3345/cep.2021.01326).
- [4] S. K. Samal et al., "3D-printed satellite brackets: Materials, manufacturing and applications," *Crystals*, vol. 12, no. 8, pp. 1–22, Aug. 2022, doi: [10.3390/cryst12081148](https://doi.org/10.3390/cryst12081148).
- [5] L. Periasamy and A. J. Gasiewski, "Prelaunch performance of the 118.75 GHz polarcube 3U cubesat temperature sounding radiometer," in *Proc. IEEE Int. Geosci. Remote Sens. Symp.*, 2018, pp. 6316–6319.
- [6] S. K. Rao, "Advanced antenna technologies for satellite communications payloads," *IEEE Trans. Antennas Propag.*, vol. 63, no. 4, pp. 1205–1217, Apr. 2015, doi: [10.1109/TAP.2015.2391283](https://doi.org/10.1109/TAP.2015.2391283).
- [7] H. Fenech, S. Amos, A. Hirsch, and V. Soumpholphakdy, "VHTS systems: Requirements and evolution," in *Proc. 11th Eur. Conf. Antennas Propag.*, 2017, pp. 2409–2412.
- [8] B. Palacin et al., "Multibeam antennas for very high throughput satellites in Europe: Technologies and trends," in *Proc. 11th Eur. Conf. Antennas Propag.*, 2017, pp. 2413–2417.
- [9] N. J. G. Fonseca, J.-C. Angevain, and C. Manganot, "Toward the Terabit/s satellite: Antenna design trade-offs and analyses," in *Proc. 33rd ESA Antenna Workshop*, Noordwijk, The Netherlands, Oct. 2011, pp. 1–8.
- [10] Y. Demers et al., "Ka-band user antennas for VHTS GEO applications," in *Proc. 11th Eur. Conf. Antennas Propag.*, 2017, pp. 2418–2422.
- [11] R. Baroni et al., "Performance analysis of a mesh satellite system based on linear and continuous phase modulations," in *Proc. IEEE Int. Conf. Commun.*, 2012, pp. 3255–3259.
- [12] A. Gharanjik, B. Shankar M. R., P.-D. Arapoglou, and B. Ottersten, "Multiple gateway transmit diversity in Q/V band feeder links," *IEEE Trans. Commun.*, vol. 63, no. 3, pp. 916–926, Mar. 2015, doi: [10.1109/TCOMM.2014.2385703](https://doi.org/10.1109/TCOMM.2014.2385703).
- [13] N. J. G. Fonseca and J. Sombrin, "Multi-beam reflector antenna system combining beam hopping and size reduction of effectively used spots," *IEEE Antennas Propag. Mag.*, vol. 54, no. 2, pp. 88–99, Apr. 2012, doi: [10.1109/MAP.2012.6230720](https://doi.org/10.1109/MAP.2012.6230720).
- [14] J. Hill, Y. Demers, A. Liang, É. Amyotte, K. Glâtre, and S. Richard, "Multibeam antenna architectures for flexible capacity allocation," in *Proc. 39th ESA Antenna Workshop Innov. Antenna Syst. Technol. Future Space Missions*, Noordwijk, The Netherlands, Oct. 2018, pp. 1–8.
- [15] E. Calà, M. Baldelli, A. Catalani, E. Menargues, G. Toso, and P. Angeletti, "Development of a Ka-band non-regular multibeam coverage antenna," *IEEE Trans. Antennas Propag.*, vol. 71, no. 1, pp. 7–17, Jan. 2023, doi: [10.1109/TAP.2022.3217890](https://doi.org/10.1109/TAP.2022.3217890).
- [16] M. Schneider, C. Hartwanger, and H. Wolf, "Antennas for multiple spot beam satellites," *CEAS Space J.*, vol. 2, pp. 59–66, Dec. 2011, doi: [10.1007/s12567-011-0012-z](https://doi.org/10.1007/s12567-011-0012-z).
- [17] M. Cooley, "Phased array fed reflector (PAFR) antenna architectures for space-based sensors," in *Proc. IEEE Aerosp. Conf.*, 2015, pp. 1–11, doi: [10.1109/AERO.2015.7118963](https://doi.org/10.1109/AERO.2015.7118963).

- [18] A. Baldominos, A. Segneri, A. Mengali, N. J. G. Fonseca, and G. Goussetis, "Comparative study of beamforming techniques for VHTS array fed reflector antennas," in *Proc. 16th Eur. Conf. Antennas Propag.*, 2022, pp. 1–5.
- [19] A. I. Perez-Neira, M. A. Vazquez, M. R. B. Shankar, S. Maleki, and S. Chatzinotas, "Signal processing for high-throughput satellites: Challenges in new interference-limited scenarios," *IEEE Signal Process. Mag.*, vol. 36, no. 4, pp. 112–131, Jul. 2019, doi: [10.1109/MSP.2019.2894391](https://doi.org/10.1109/MSP.2019.2894391).
- [20] N. J. G. Fonseca et al., "Satellite antenna technologies enabling 5G mobile direct services," in *Proc. 17th Eur. Conf. Antennas Propag.*, Florence, Italy, Mar. 2023, pp. 1–5.
- [21] J.-C. Angevain, A. Ihle, G. Rodrigues, and J. Santiago-Prowald, "Large deployable spaceborne reflector antennas in Europe: Progress status and perspectives," in *Proc. 13th Eur. Conf. Antennas Propag.*, 2019, pp. 1–5.
- [22] O. B. Osoro and E. J. Oughton, "A techno-economic framework for satellite networks applied to low Earth orbit constellations: Assessing Starlink, OneWeb and Kuiper," *IEEE Access*, vol. 9, pp. 141611–141625, 2021, doi: [10.1109/ACCESS.2021.3119634](https://doi.org/10.1109/ACCESS.2021.3119634).
- [23] K. Glatre, L. Hildebrand, E. Charbonneau, J. Perrin, and E. Amyotte, "Paving the way for higher-volume cost-effective space antennas: Designing for manufacturing assembly integration and test," *IEEE Antennas Propag. Mag.*, vol. 61, no. 5, pp. 47–53, Oct. 2019, doi: [10.1109/MAP.2019.2932313](https://doi.org/10.1109/MAP.2019.2932313).
- [24] I. Gibson, D. W. Rosen, and B. Stucker, *Additive Manufacturing Technologies: Rapid Prototyping to Direct Digital Manufacturing*. New York, NY, USA: Springer, 2010.
- [25] ASTM-F2792-12a, "Standard terminology for additive manufacturing technologies," in *ASTM International*. West Conshohocken, PA, USA: ASTM, 2012, pp. 1–3.
- [26] M. Lumia, G. Addamo, O. A. Peverini, F. Calignano, G. Virone, and D. Manfredi, "Additive manufacturing of RF waveguide components," in *Recent Microwave Technologies*. London, U.K.: IntechOpen, 2022, pp. 1–21, doi: [10.5772/intechopen.104106](https://doi.org/10.5772/intechopen.104106).
- [27] F. Calignano et al., "Overview on additive manufacturing technologies," *Proc. IEEE*, vol. 105, no. 4, pp. 593–612, Apr. 2017, doi: [10.1109/JPROC.2016.2625098](https://doi.org/10.1109/JPROC.2016.2625098).
- [28] C. R. Garcia, R. C. Rumpf, H. H. Tsang, and J. H. Barton, "Effects of extreme surface roughness on 3D printed horn antenna," *Electron. Lett.*, vol. 49, no. 12, pp. 734–736, Jun. 2013, doi: [10.1049/el.2013.1528](https://doi.org/10.1049/el.2013.1528).
- [29] B. Zhang, Y.-X. Guo, H. Zirath, and Y. P. Zhang, "Investigation on 3-D-printing technologies for millimeter-wave and terahertz applications," *Proc. IEEE*, vol. 105, no. 4, pp. 723–736, Apr. 2017, doi: [10.1109/JPROC.2016.2639520](https://doi.org/10.1109/JPROC.2016.2639520).
- [30] S. Sirci, E. Menargues, and M. Billod, "Space-qualified additive manufacturing and its application to active antenna harmonic filters," in *Proc. IEEE MTT-S Int. Microw. Filter Workshop*, 2021, pp. 239–242.
- [31] F. Calignano, O. A. Peverini, G. Addamo, and L. Iuliano, "Accuracy of complex internal channels produced by laser powder bed fusion process," *J. Manufact. Processes*, vol. 54, pp. 48–53, Jun. 2020, doi: [10.1016/j.jmapro.2020.02.045](https://doi.org/10.1016/j.jmapro.2020.02.045).
- [32] O. A. Peverini et al., "Additive manufacturing of Ku/K-band waveguide filters: A comparative analysis among selective-laser melting and stereo-lithography," *IET Microw. Antennas Propag.*, vol. 11, no. 14, pp. 1936–1942, Sep. 2017, doi: [10.1049/iet-map.2017.0151](https://doi.org/10.1049/iet-map.2017.0151).
- [33] G. Addamo et al., "Additive manufacturing of Ka-band dual-polarization waveguide components," *IEEE Trans. Microw. Theory Techn.*, vol. 66, no. 8, pp. 3589–3596, Aug. 2018, doi: [10.1109/TMTT.2018.2854187](https://doi.org/10.1109/TMTT.2018.2854187).
- [34] K. Lomakin, M. Sippel, K. Helmreich, and G. Gold, "Design and analysis of 3D printed slotted waveguides for D-band using stereolithography and electroless silver plating," in *Proc. IEEE/MTT-S Int. Microw. Symp.*, 2020, pp. 177–180.
- [35] J. Shen, M. Aiken, C. Ladd, M. D. Dickey, and D. S. Ricketts, "A simple electroless plating solution for 3D printed microwave components," in *Proc. Asia-Pacific Microw. Conf.*, 2016, pp. 1–4.
- [36] M. Dionigi, C. Tomassoni, G. Venanzoni, and R. Sorrentino, "Simple high-performance metal-plating procedure for stereolithographically 3-D-printed waveguide components," *IEEE Microw. Wireless Compon. Lett.*, vol. 27, no. 11, pp. 953–955, Nov. 2017, doi: [10.1109/LMWC.2017.2750090](https://doi.org/10.1109/LMWC.2017.2750090).
- [37] J. Shen et al., "Rapid prototyping of low loss 3D printed waveguides for millimeter-wave applications," in *Proc. IEEE MTT-S Int. Microw. Symp.*, 2017, pp. 41–44.
- [38] K. Fujiwara, R. Kobayashi, S. Kuwahara, S. Takemura, K. Takizawa, and Y. Watanabe, "3-D printed iris waveguide filter in W-band," in *Proc. 23rd Int. Microw. Radar Conf.*, 2020, pp. 346–349.
- [39] F. Calignano, D. Manfredi, E. P. Ambrosio, L. Iuliano, and P. Fino, "Influence of process parameters on surface roughness of aluminum parts produced by DMLS," *Int. J. Adv. Manuf. Technol.*, vol. 67, pp. 2743–2751, 2013, doi: [10.1007/s00170-012-4688-9](https://doi.org/10.1007/s00170-012-4688-9).
- [40] A. I. Dimitriadis et al., "Polymer-based additive manufacturing of high-performance waveguide and antenna components," *Proc. IEEE*, vol. 105, no. 4, pp. 668–676, Apr. 2017, doi: [10.1109/JPROC.2016.2629511](https://doi.org/10.1109/JPROC.2016.2629511).
- [41] P. Martín-Iglesias, M. van der Vorst, J. Gumpinger, and T. Ghidini, "ESA's recent developments in the field of 3D-printed RF/microwave hardware," in *Proc. 11th Eur. Conf. Antennas Propag.*, 2017, pp. 553–557.
- [42] M. Kilian, C. Hartwanger, M. Schneider, and M. Hatzebichler, "Waveguide components for space applications manufactured by additive manufacturing technology," *IET Microw. Antennas Propag.*, vol. 11, no. 14, pp. 1949–1954, Nov. 2017, doi: [10.1049/iet-map.2016.0984](https://doi.org/10.1049/iet-map.2016.0984).
- [43] P. Martín-Iglesias et al., "Metal 3D printing for RF/microwave high-frequency parts," *CEAS Space J.*, vol. 15, pp. 7–25, 2023, doi: [10.1007/s12567-022-00447-y](https://doi.org/10.1007/s12567-022-00447-y).
- [44] C. Bachiller, V. Nova, Á. Ferrer, and V. E. B. Esbert, "Space qualification of metalized additive manufactured filters," *IEEE Access*, vol. 10, pp. 96952–96966, 2022, doi: [10.1109/ACCESS.2022.3205408](https://doi.org/10.1109/ACCESS.2022.3205408).
- [45] R. G. Edwards, C. M. Norton, J. E. Campbell, and D. Schurig, "Effective conductivity of additive-manufactured metals for microwave feed components," *IEEE Access*, vol. 9, pp. 59979–59986, 2021, doi: [10.1109/ACCESS.2021.3071486](https://doi.org/10.1109/ACCESS.2021.3071486).
- [46] L. Polo-López et al., "Waveguide manufacturing technologies for next-generation millimeter-wave antennas," *Micromachines*, vol. 12, no. 12, Dec. 2021, Art. no. 1565, doi: [10.3390/mi12121565](https://doi.org/10.3390/mi12121565).
- [47] M. Kilian, C. Hartwanger, and M. Schneider, "RF feed chain components manufactured by additive manufacturing techniques," in *Proc. IEEE Int. Conf. Electromagn. Adv. Appl.*, 2017, pp. 555–558.
- [48] C. Youssef et al., "Ku-band lightweight aluminium waveguides fabricated by direct metal laser sintering process," in *Proc. Int. Symp. Adv. Elect. Commun. Technol.*, 2020, pp. 1–4.
- [49] J. A. Lorente, M. M. Mendoza, A. Z. Petersson, L. Pambaguian, A. A. Melcon, and C. Ernst, "Single part microwave filters made from selective laser melting," in *Proc. Eur. Microw. Conf.*, 2009, pp. 1421–1424.
- [50] P. A. Booth and E. V. Lluch, "Realising advanced waveguide bandpass filters using additive manufacturing," *IET Microw. Antennas Propag.*, vol. 11, no. 14, pp. 1943–1948, Oct. 2017, doi: [10.1049/iet-map.2017.0170](https://doi.org/10.1049/iet-map.2017.0170).
- [51] P. Booth, "Additive manufactured bandpass filters at Ka-band," in *Proc. IEEE MTT-S Int. Microw. Workshop Ser. Adv. Mater. Processes RF THz Appl.*, 2019, pp. 7–9.
- [52] M. M. Mendoza, S. Sobrino, A. I. Daganzo, T. Debogovic, M. Favre, and E. de Rijk, "Electrical tests of Ka band input filters for space applications," in *Proc. 11th Eur. Conf. Antennas Propag.*, 2017.
- [53] O. A. Peverini et al., "Selective laser melting manufacturing of microwave waveguide devices," *Proc. IEEE*, vol. 105, no. 4, pp. 620–631, Apr. 2017, doi: [10.1109/JPROC.2016.2620148](https://doi.org/10.1109/JPROC.2016.2620148).
- [54] L. Polo-López et al., "Vertically printable evanescent mode filters," *IEEE Microw. Wireless Compon. Lett.*, vol. 32, no. 11, pp. 1299–1302, Nov. 2022, doi: [10.1109/LMWC.2022.3187781](https://doi.org/10.1109/LMWC.2022.3187781).
- [55] P. Booth, J. Gilmore, E. V. Lluch, and M. Harvey, "Enhancements to satellite feed chain performance, testing and lead-times using additive manufacturing," in *Proc. 10th Eur. Conf. Antennas Propag.*, 2016, pp. 1–5.
- [56] P. Booth, M. Skeen, and S. Stirland, "Low cost, short lead-time feed chain components for multi-beam antennas," in *Proc. 3rd Eur. Conf. Antennas Propag.*, 2009, pp. 853–857.
- [57] P. Kohl, M. Kilian, A. Schinagl-Weiß, and C. Hartwanger, "Additive manufacturing developments for satellite antenna applications from C-to Ka-band," in *Proc. 12th German Microw. Conf.*, 2019, pp. 222–225.
- [58] M. Kilian, M. Schneider, P. Kohl, and C. Hartwanger, "Feasibility study for dual septum polarisers manufactured by additive layer manufacturing," in *Proc. IEEE 14th German Microw. Conf.*, 2022, pp. 124–127.
- [59] E. Menargues et al., "Compact orthomode transducer with broadband beamforming capability," in *Proc. IEEE MTT-S Int. Microw. Symp.*, 2018, pp. 152–155.

- [60] J. Fordham, E. Barry, R. Burge, M. Hollenbeck, and R. Smith, "Additive manufactured 3:1 bandwidth dual-polarized range antenna," in *Proc. Antenna Meas. Techn. Assoc. Symp.*, 2020, pp. 1–6.
- [61] L. Polo-López, E. Menargues, S. Capdevila, G. Toso, and M. García-Vigueras, "Solving sub-wavelength lattice reduction in full-metal front-ends for dual-polarized active antennas," *IEEE Trans. Antennas Propag.*, vol. 70, no. 9, pp. 7413–7426, Sep. 2022, doi: [10.1109/TAP.2022.3198512](https://doi.org/10.1109/TAP.2022.3198512).
- [62] G. Addamo et al., "3-D Printing of high-performance feed horns from Ku- to V-bands," *IEEE Antennas Wireless Propag. Lett.*, vol. 17, no. 11, pp. 2036–2040, Nov. 2018, doi: [10.1109/LAWP.2018.2859828](https://doi.org/10.1109/LAWP.2018.2859828).
- [63] C. Stoumpos, J.-A. Duran-Venegas, T. Pierré, and M. García-Vigueras, "Multipactor analysis of high-power Ku-band orthomode transducers (OMTs) in aluminum selective laser melting (SLM)," in *Proc. 10th Int. Workshop Multipactor Corona Passive Intermodulation Space RF Hardware*, Valencia, Spain, Oct. 2022, pp. 1–7.
- [64] P. Martín-Iglesias et al., "Enhanced multipactor performance in 3D printed microwave parts," in *Proc. IEEE MTT-S Int. Microw. Workshop Ser. Adv. Mater. Processes RF THz Appl.*, 2017, pp. 1–3.
- [65] Y. Cailloce, P. Hourlay, F. Lebrun, and B. Palacin, "Additive manufacturing of Ku band horn antennas for telecommunications space applications," in *Proc. 12th Eur. Conf. Antennas Propag.*, 2018, pp. 1–4.
- [66] J. Rico-Fernández, F. V. Vidarsson, M. Arrebola, N. J. G. Fonseca, and O. Quevedo-Teruel, "Compact and lightweight additive manufactured parallel-plate waveguide half-Luneburg geodesic lens multiple-beam antenna in the Ka-band," *IEEE Antennas Wireless Propag. Lett.*, early access, Nov. 15, 2022, doi: [10.1109/LAWP.2022.3222172](https://doi.org/10.1109/LAWP.2022.3222172).
- [67] S. Sirci, E. Menargues, and S. Berry, "Triangular combline filters conceived for additive manufacturing," in *Proc. IEEE MTT-S Int. Microw. Filter Workshop*, 2021, pp. 151–154.
- [68] C. Tomassoni, O. A. Peverini, G. Venanzoni, G. Addamo, F. Paonessa, and G. Virone, "3D printing of microwave and millimeter-wave filters: Additive manufacturing technologies applied in the development of high-performance filters with novel topologies," *IEEE Microw. Mag.*, vol. 21, no. 6, pp. 24–45, Jun. 2020, doi: [10.1109/MMM.2020.2979153](https://doi.org/10.1109/MMM.2020.2979153).
- [69] X. Cheng et al., "Analysis and design of a wideband endfire circularly polarized septum antenna," *IEEE Trans. Antennas Propag.*, vol. 66, no. 11, pp. 5783–5793, Nov. 2018, doi: [10.1109/TAP.2018.2866584](https://doi.org/10.1109/TAP.2018.2866584).
- [70] M. Kilian, A. Schinagl-Weiss, P. Kohl, A. Sommer, C. Hartwanger, and M. Schneider, "Additive layer manufactured waveguide RF components," in *Proc. 49th Eur. Microw. Conf.*, 2019, pp. 790–793.
- [71] O. A. Peverini et al., "Integration of an H-plane bend, a twist, and a filter in Ku/Ka-band through additive manufacturing," *IEEE Trans. Microw. Theory Techn.*, vol. 66, no. 5, pp. 2210–2219, May 2018, doi: [10.1109/TMTT.2018.2809505](https://doi.org/10.1109/TMTT.2018.2809505).
- [72] C. Wang, J. Wu, B. Ma, and Y. Guo, "A 3D-printed K/Ka-band dual circularly polarized feed for offset-fed reflector antennas," in *Proc. IEEE Asia-Pacific Microw. Conf.*, 2020, pp. 558–560.
- [73] B. Zhang, R. Li, L. Wu, H. Sun, and Y.-X. Guo, "A highly integrated 3-D printed metallic K-band passive front end as the unit cell in a large array for satellite communication," *IEEE Antennas Wireless Propag. Lett.*, vol. 17, no. 11, pp. 2046–2050, Nov. 2018, doi: [10.1109/LAWP.2018.2824298](https://doi.org/10.1109/LAWP.2018.2824298).
- [74] M. Hollenbeck, R. Smith, C. Cathey, and J. Opra, "X-band integrated printed antenna measurement," in *Proc. IEEE MTT-S Int. Microw. Symp.*, 2018, pp. 149–151.
- [75] M. Kilian, P. Kohl, C. Hartwanger, and M. Schneider, "High gain Ka band ALM feed chain," in *Proc. IEEE MTT-S Int. Microw. Workshop Ser. Adv. Mater. Processes RF THz Appl.*, 2019, pp. 37–39.
- [76] G. Addamo et al., "3D Printing of a monolithic K/Ka-band dual-circular polarization antenna-feeding network," *IEEE Access*, vol. 9, pp. 88243–88255, 2021, doi: [10.1109/ACCESS.2021.3089826](https://doi.org/10.1109/ACCESS.2021.3089826).
- [77] J.-G. Gong, Q. Li, M.-T. Zhang, J. Hou, Y. Wang, and Z. Xu, "A wide-band dual circular polarization feed chain for satellite antennas at K/Ka bands," in *Proc. Prog. Electromagn. Res. Symp.*, 2017, pp. 222–226.
- [78] N. J. G. Fonseca and J.-C. Angevain, "Waveguide hybrid septum coupler," *IEEE Trans. Microw. Theory Techn.*, vol. 69, no. 6, pp. 3030–3036, Jun. 2021, doi: [10.1109/TMTT.2021.3074194](https://doi.org/10.1109/TMTT.2021.3074194).
- [79] P. Bosshard et al., "Thales Alenia Space HTS/V-HTS multiple beam antennas sub-systems on the right track," in *Proc. 10th Eur. Conf. Antennas Propag.*, 2016, pp. 1–5.
- [80] N. J. G. Fonseca, "Two-probe waveguide orthomode transducer with twofold rotational symmetry," *IEEE Trans. Microw. Theory Techn.*, vol. 69, no. 7, pp. 3228–3235, Jul. 2021, doi: [10.1109/TMTT.2021.3075957](https://doi.org/10.1109/TMTT.2021.3075957).
- [81] A. Sommer, A. Schinagl-Weiß, C. Hartwanger, M. Kilian, and M. Schneider, "Multiple spot beam reflector antenna for high throughput satellites using additive manufacturing technology," in *Proc. 13th Eur. Conf. Antennas Propag.*, 2019, pp. 1–5.
- [82] M. Kilian, A. Schinagl-Weiß, A. Sommer, C. Hartwanger, and M. Schneider, "Ku-band SFB-cluster manufactured by additive manufacturing techniques," in *Proc. IEEE 13th Eur. Conf. Antennas Propag.*, 2019, pp. 1–4.



OSCAR A. PEVERINI (Member, IEEE) was born in Lisbon, Portugal, in April 1972. He received the Laurea degree (*summa cum laudae*) in telecommunication engineering and the Ph.D. degree in electronic engineering from the Politecnico di Torino, Turin, Italy, in 1997 and 2001, respectively. During his postdoctoral studies, he was a Visiting Researcher with the University of Paderborn, Paderborn, Germany, where he was involved in the design of acousto-optical devices. In 2001, he was a Research Fellow with the Physics Department, Politecnico di Torino, and IRITI Institute of the National Research Council of Italy (CNR). In December 2001, he joined CNR-IEIIT institute, where he is currently a Director of Research and the coordinator of the Applied Electromagnetics and Electronic Devices Research Unit. Since 2015, he has been a Research Associate with Italian Space Agency. He is the Technical Manager of several projects aimed at the development of microwave and millimeter-wave devices for space-born applications. He is a reviewer of several journals and conferences in the microwave area. He has authored or coauthored more than 50 journal articles, 110 conference papers, and he is a co-inventor of three European patents. From 2018 to 2021, he was the President of the Evaluation Board for the Research and Development Projects submitted in the ICT area within the calls of the Fund for Sustainable Growth Programme of the Italian Ministry of Economic Development.



MAURO LUMIA (Member, IEEE) was born in Torino, Italy, in February 1983. He received the master's degree in mechanical engineering and the Ph.D. degree in electronic engineering from the Politecnico di Torino, Turin, Italy, in 2012 and 2017, respectively. In 2013, he joined the Applied Electromagnetics and Electronic Devices Group, CNR-IEIIT, as a Research Fellow, where he is currently a Researcher. His primary research interests include research on the manufacturing processes for waveguide components with a focus on additive manufacturing technologies.



GIUSEPPE ADDAMO (Member, IEEE) was born in Messina, Italy, in 1979. He received the Laurea degree (*summa cum laude*) in electronic engineering and the Ph.D. degree in electronic and communication engineering from the Politecnico di Torino, Turin, Italy, in 2003 and 2007, respectively. In 2007, he joined the Italian National Research Council (CNR), Institute of Electronics, Computer and Telecommunication Engineering (IEIIT), Turin, as a Research Fellow, where he became a Researcher in 2012. He holds practical classes in courses on electromagnetic field theory and mathematical analysis with the Politecnico di Torino. His research interests include the design of feed chain for SatCom and Earth Observation, corrugated and smooth wall horn, microwave leaky antennas, frequency-selective surfaces, and large dielectric radomes.



GIUSEPPE VIRONE (Senior Member, IEEE) was born in Turin, Italy, in 1977. He received the Degree in electronic engineering (*summa cum laude*, November 2001) and the Ph.D. degree in electronics and communication engineering in 2006 both from the Politecnico di Torino, Turin, Italy. He is currently a Senior Researcher with the Istituto di Elettronica e di Ingegneria Informatica e delle Telecomunicazioni, Italian National Research Council (CNR). In 2002, he joined IEIIT as a Research Assistant. He coordinated more than 15

scientific projects funded by both the industry and other scientific research organizations and joined more than 30 research projects as a collaborator. He authored 43 journal papers, 134 conference papers and three European patents. His activities concern the design, numerical analysis and characterization of microwave and millimeter passive components for feed systems, antenna arrays, frequency selective surfaces, compensated dielectric radomes, and industrial sensing applications.



NELSON J. G. FONSECA (Senior Member, IEEE) received the M.Eng. degree in electrical engineering from the Ecole Nationale Supérieure d'Electrotechnique, Electronique, Informatique, Hydraulique et Télécommunications, Toulouse, France, in 2003, the M.Sc. degree in electrical engineering from the Ecole Polytechnique de Montreal, Quebec, Canada, in 2003, and the Ph.D. degree in electrical engineering from the Institut National Polytechnique de Toulouse – Université de Toulouse, France, in 2010.

He is currently an Antenna Engineer with the Antenna and Sub-Millimeter Waves Section, European Space Agency (ESA), Noordwijk, The Netherlands. Since November 2020, he also holds an Honorary Appointment as Professional Fellow with the University of Technology Sydney (UTS), Ultimo, NSW, Australia. He has authored or coauthored more than 290 papers in peer-reviewed journals and conferences and has more than 50 patents issued or pending. His research interests include multiple beam antennas for space missions, beam-former theory and design, ground terminal antennas, transfer of technology to and from terrestrial systems, including 5G networks, and novel manufacturing techniques.

Dr. Fonseca is the Chair of the newly founded IEEE MTT-S Technical Committee 29 on Microwave Aerospace Systems. Since January 2019, he has been a Board Member of the European School of Antennas (ESoA) and is actively involved both as a Lecturer and as coordinator in courses related to space and ground antennas. He is the elected EurAAP Regional Delegate representing Benelux for the term, from 2021 to 2023. He was an Associate Editor for IEEE TRANSACTIONS ON MICROWAVE THEORY AND TECHNIQUES from 2020 to 2022 and the Guest Editor of two Focused Issues on Aerospace Applications for the *IEEE Microwave Magazine* in 2022 and 2023. He is also an Associate Editor for IEEE TRANSACTIONS ON ANTENNAS AND PROPAGATION and *IET Microwaves, Antennas and Propagations*, and a Topic Editor of IEEE JOURNAL OF MICROWAVES.

Open Access funding provided by 'Consiglio Nazionale delle Ricerche-CARI-CARE' within the CRUI CARE Agreement